

ChemSICal-Net: Timing-Controlled Chemical Reaction Network for Successive Interference Cancellation in Molecular Multiple Access

Alexander Wietfeld, *Graduate Student Member, IEEE*, Oguz Turgut, Eneritz Somoza Rodríguez, Wolfgang Kellerer, *Fellow, IEEE*

Abstract—Molecular communication (MC) networks are envisioned to enable synthetic information exchange between nanoscale biological entities. For many algorithm proposals in the MC research field, the question of implementation at nanoscales and in biological environments remains open. Chemical reaction networks (CRNs) provide a natural framework to model computing processes in biological systems, while detailed simulations capture realistic stochastic effects. In this work, we present ChemSICal-Net, a comprehensive CRN simulation model of a chemical receiver implementing successive interference cancellation (SIC) to differentiate messages from multiple transmitters. We present the structure of the SIC algorithm in the form of basic chemical building blocks and incorporate clocked timing control by a chemical oscillator. We propose an adaptive Bayesian optimization (BO) scheme with a Gaussian process surrogate to find appropriate values for the reaction rate constants and the initial concentrations and show that it outperforms baseline methods from related work based on a fair computational cost metric. Then, the performance of the ChemSICal-Net framework is evaluated stochastically across a range of clock speeds and in different configurations focusing on communication system metrics such as detection accuracy and decision time. Our results highlight that the timing via a chemical clock can improve the detection accuracy by a factor of 2 in scenarios with shorter decision times, which underlines how the trade-off between decision time and detection probability can shape CRN design choices. The BO scheme is shown to reliably optimize parameters for different configurations by approximately one order of magnitude compared to the non-optimized case. Our system reveals the need for a multi-scale approach with external BO and stochastic simulation of molecular reaction dynamics for communication-metric-focused system design.

Index Terms—Molecular communication, chemical reaction networks, NOMA, successive interference cancellation, chemical oscillator, Bayesian optimization

I. INTRODUCTION

MOLECULAR communication (MC) is defined as the information transfer using molecules [1]. As a bio-compatible and energy-efficient alternative to classical electromagnetic signals, diffusion-based molecular communication (DBMC) [2] will play a major role in a future Internet of

Bio-Nano-Things (IoBNT), connecting bio-nano nodes inside the human body [3]. Recent advances in bio-nanotechnology and micro-robotics have shown that monitoring and targeted interventions have the potential to enable novel medical use cases [4], but still require external tools and human operation.

Biological devices at small scales, so-called Bio-Nano-Machines (BNMs), will offer severely limited communication capabilities and computing resources [5]. To realize the IoBNT vision, autonomous networked systems and novel computing approaches are needed to connect multiple BNMs and implement more complex decision mechanisms. As a result, multi-user communication becomes an important reference case, for example, where multiple transmitters (TXs) report to a shared receiver (RX) for data gathering [6]. Interference management and avoidance is crucial when multiple transmissions need to be coordinated. Therefore, molecular multiple access (MA) has received significant attention, including orthogonal and non-orthogonal approaches relying on procedures and algorithms such as successive interference cancellation (SIC) [6]–[8]. However, most MA schemes for DBMC are evaluated at the level of abstract RX models and typically assume digital processing resources that do not exist in BNMs to execute algorithms.

This gap motivates research into chemical implementations of signal processing and computing. Chemical reaction networks (CRNs) are combinations of chemical reactions that by specific coupling of reactants and products of different reactions enable the implementation of simple mathematical and logical functions [9]. As a consequence, they have become a promising substrate for TX and RX functionality in DBMC networks both in experiments [10], [11], as well as simulation studies [12]. Recent work suggests that CRNs provide a credible path toward algorithm implementation without relying on electronic and digital components in biological environments. Therefore, proposed algorithms must be robust under the influence of chemical dynamics and inherent stochasticity of CRNs [12].

In this context, we introduced ChemSICal as a stochastic CRN simulation model of SIC for non-orthogonal multiple access (NOMA) in DBMC networks [13], performed a preliminary evaluation and investigated how chemical parameters like reaction rate constants (RRCs) influenced performance. Building on this foundation, the goal of this paper is to advance from a standalone CRN SIC implementation toward a full RX system that adds two crucial missing aspects: explicit

The authors acknowledge the financial support by the German Federal Ministry of Research, Technology and Space (BMFTR) in the program of “Souverän. Digital. Vernetzt!”. Joint project 6G-life, project identification number: 16KISK002.

Alexander Wietfeld and Wolfgang Kellerer are with the Chair of Communication Networks, Technical University of Munich, 80333 Munich, Germany (e-mail: {alexander.wietfeld, wolfgang.kellerer}@tum.de). Oguz Turgut and Eneritz Somoza Rodríguez were with the Chair of Communication Networks, Technical University of Munich, 80333 Munich, Germany, at the time this work was conducted.

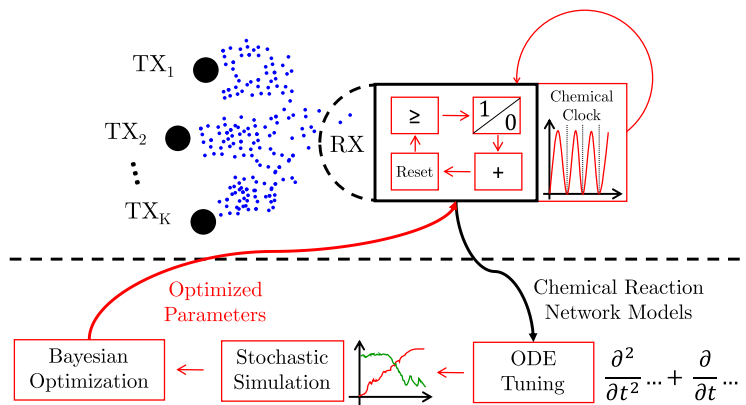


Fig. 1: Schematic representation of the ChemSICal-Net framework, showing the DBMC channel with multiple transmitters, and the receiver with block-based chemical computing operations and chemical clock for timing. We showcase the multi-scale design loop: The system can be expressed as ordinary differential equation (ODE), which can be used for initial parameter tuning. Then, comprehensive stochastic simulations form the input for our proposed Bayesian optimization (BO) scheme.

timing control of multi-stage processing using a chemical oscillator, and systematic optimization in high-dimensional CRN parameter spaces.

We address how a chemical SIC RX can be realized as a CRN connected to a DBMC channel with dynamic inputs [13] and evaluate the system thoroughly with ordinary differential equation (ODE) solvers and stochastic simulations. Further, we ask how a chemical timing process can be integrated into the multi-TX SIC algorithm to gate different stages and make the decision and readout timing an explicit design parameter. We investigate the conditions under which the chemical timing can improve performance via added control, or when the added reaction complexity can degrade performance compared to the non-timed version. Finally, we investigate how Bayesian optimization (BO), which has a proven track record for usage in complex chemical systems [14]–[16], can be adapted to tune constrained stochastic CRNs with communication-centric metrics such as error probability. The resulting *ChemSICal-Net* framework targets an end-to-end view of a chemical SIC RX as a DBMC system component and includes modular proof-of-concept components toward reuse through a reset mechanism and scaling beyond two simultaneous TXs. An overview of the proposed concept can be seen in Figure 1.

A. State of the Art

In the following, the state-of-the-art in relevant research areas will be summarized and relevant gaps highlighted. This includes MA for DBMC networks, CRNs for modeling chemical algorithms, using chemical oscillators to control CRN algorithms, and BO for chemical reaction tuning.

1) Multiple access in DBMC networks

MA schemes have been explored extensively in DBMC literature as one of the first important steps towards multi-node networks. One main category covers orthogonal approaches such as time-division multiple access (TDMA) [6], where each TX is assigned a specific time slot, or molecule-division multiple access (MDMA) [17], which involves different molecule types per TX that can be chemically differentiated at the RX. Advanced approaches exist, for example, using molecule mixtures for MDMA, inspired by olfactory systems [18].

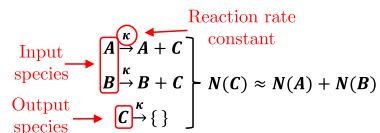


Fig. 2: Example of a simple CRN computing the sum of the molecule counts of two input species A and B as the molecule count of a third chemical species C.

While orthogonal approaches inherently reduce interference, they incur different types of overhead, such as strict timing requirements and a lack of simultaneous transmissions for TDMA, or increased chemical complexity through required compatibility of TX and RX with additional molecule species for MDMA. NOMA-inspired approaches have been explored recently [7], [8] to allow for simultaneous transmission from multiple TXs with the same molecule type. Similar concepts have been shown to be successful at increasing capacity in classical communication networks [19]. In the most common form, power-domain NOMA, the RX experiences additional interference from simultaneously transmitting TXs, which can be mitigated using a SIC algorithm based on differences in received signal strength [20].

The most prevalent style of evaluation for DBMC MA literature remains based on abstract RX models. This has revealed important insights about performance and design trade-offs between different MA schemes [8], but the realization of the necessary algorithms, for example, for synchronization, coding, or SIC in bio-nano environments is still largely unaddressed. Despite the maturity of the research area, this leaves an open gap regarding the realistic modeling of MA scheme implementations in DBMC networks without generic digital computing capabilities.

2) CRNs for computing in DBMC networks

A chemical reaction is defined by molecule species inputs (reactants), molecule species outputs (products) and the speed of the reaction between them (RRCs). Figure 2 shows an example of a CRN, in which multiple chemical reactions interact to implement a simple mathematical addition function. Research into molecular programming frameworks has

shown that CRNs offer an appropriate modeling substrate for chemical computing using reaction blocks that enable further operations like comparisons or multiplication [9]. Heinlein et al. have recently proposed the first CRN-based DBMC RX that includes symbol detection and synchronization for single-link communication [12]. Other related work has considered CRN-like building blocks and precise interplay of reaction volumes to create simple neural network structures in the chemical domain [21]. In addition, recent work has highlighted the specific role of DNA-based reactions for the implementation of programmable molecular protocols [22], as well as experimental DBMC systems [23].

These papers establish that chemical computation and DBMC-node signal processing using CRNs is possible and promising in principle, and experimental work has shown artificial cells can act as chemical reactors containing CRN processes [5]. However, remaining challenges are the integration of CRN-based algorithms into multi-user networks, the connection with a dynamic DBMC channel, and the evaluation using communication metrics and stochastic simulations. While some works address CRNs using stochastic simulations [12], they lack the multi-user network aspect, and other consider more complex protocols [22], but do not integrate the system into a diffusion channel and communication-focused evaluation.

3) *Chemical oscillators for timing control*

Using chemical oscillators to control the flow of CRNs has long been a topic of research. Prior work has already proposed clocked schemes that enable sequential computation, where oscillatory signals gate certain reaction blocks one by one [24], [25]. While early work makes use of simplified oscillator models, recent work has specifically framed chemical oscillators as clock signals to be optimized for chemical computation and tuned parameters and oscillator structure to achieve properties such as symmetry [26]. While the previous papers target *toy model* oscillators, which do not exist in natural systems, the biological literature provides multiple oscillator types, including cell-cycle [27], gene-regulatory [28], or phosphorylation-driven [29] oscillations. These models represent attractive candidates, when it comes to biophysical plausibility.

The research gap consists of the use of chemical oscillators specifically for DBMC purposes with a systematic comparison of oscillator types based on clock signal metrics. Further, there is little work that connects oscillator parameter choice regarding, for example, clock frequency with communication metrics such as error probability. Lastly, most literature disregards stochastic fluctuations [30], which have a major effect on probabilistic communication performance.

4) *Bayesian optimization for stochastic CRNs*

CRN design typically involves high-dimensional parameter spaces, non-linear dynamics, and high-effort stochastic simulations, especially when the system is supposed to operate at low molecule counts and in single-cell environments [12]. Manual tuning and small-scale parameter sweeps, as have been applied in existing work on CRNs for DBMC [12], [13], [30], can provide a first intuition but do not scale to complex protocols or allow for comprehensive performance comparison. Previous work in CRN literature regarding simu-

lation models has explored different approaches to systematic optimization. Vasić et al. [31] have investigated a special class of rate-independent CRNs, which can be optimized purely with regards to stoichiometry, i.e. the numbers of molecules, as opposed to the RRCs. These networks are mostly limited to implementing piecewise-linear functions, and so the authors show how they could be useful in building neural networks with rectified linear unit function blocks.

Since complex stochastic CRN models are expensive to evaluate and usually do not allow for analytical or explicit gradient-based optimization, efficient sampling-based global optimization solutions for black-box functions are commonly employed. Murphy et al. [32] consider synthesizing CRNs for certain functions and propose a method of optimizing the reaction parameters through a Markov chain Monte Carlo (MCMC) method with a Metropolis-Hastings (MH) algorithm to estimate the posterior distribution of the parameter set from a model [33]. The method tries to bias the search towards promising regions to speed up optimization. Simulated annealing (SA) is another stochastic search scheme that explores the parameter space based on a temperature schedule allowing it to escape local minima early and later focus on gradually refining the objective as the temperature decreases [34]. Due to its general applicability to expensive objective functions, SA has been successfully applied to CRN optimization problems [35]. Lastly, Bayesian optimization (BO) tries to build a probabilistic surrogate function of the expensive black-box model and applies an acquisition rule for the next sampling point that balances exploration and exploitation [16]. BO has recently become a practical tool for efficient optimization of expensive and noisy objectives, including real-world reaction optimization under experimental constraints [14]–[16]. Therefore, it appears as a promising approach for the optimization of stochastic simulation models for CRNs.

What remains largely open is the evaluation of BO against other optimization methods as a system-level tuning mechanism for constrained stochastic CRNs in the context of DBMC objectives. Instead of chemical yield or general behavioral specifications, the objective should target metrics such as error probability or decision time. This leads to a natural multi-scale approach where the computationally heavy optimization is performed externally during design, while the deployed CRN-based DBMC system is self-contained within its constrained environment.

5) *Summary of gaps*

Across these bodies of work, a clear missing intersection emerges. Multi-user DBMC MA is well studied at the system level, and chemical RX pipelines and timing primitives exist in related contexts. However, end-to-end designs that implement multi-user SIC as a stochastic CRN, integrate an explicit chemical timing primitive, and systematically tune constrained parameters against DBMC communication objectives remain scarce.

In [13], we presented ChemSICal as the first explicit effort to map SIC into a stochastic CRN and evaluated it under DBMC channel conditions. The work demonstrated that realistic chemical models can deviate substantially from

the idealized SIC assumptions due to stochastic effects and reaction competition. At the same time, it revealed major gaps in the system integration. First, multi-stage processing in CRNs is logically sequential but physically concurrent, which makes it difficult to enforce stage boundaries and validate early-stage decisions in time. Second, it highlights the high parameter dimensionality and sensitivity that makes it hard to tune the CRN parameters manually or analytically. Lastly, the ChemSICal system is limited to 2 TXs and does not address issues with repeated use of the CRN via a reset or state-clearing mechanism.

This motivates ChemSICal-Net as a step toward network-ready chemical signal processing.

B. Contributions and extension of previous work

This work builds upon our previous work in [13] and the state of the art as described above by making several contributions:

- 1) **ChemSICal-Net: an MA-oriented chemical SIC RX framework:** We present an end-to-end CRN design that implements SIC-based multi-user reception and interfaces with DBMC channel observations. We deepen our initial analysis in [13] via comprehensive multi-scale evaluation using deterministic ODE analysis for coarse tuning and stochastic simulations for detailed performance analysis, quantifying where and how chemical models deviate from idealized assumptions.
- 2) **Clocked execution with chemical oscillator control:** Towards system integration, we incorporate a chemical timing primitive to control processing stages and make decision time a controllable design parameter. To that end, we systematically compare multiple relevant candidate oscillators [27]–[29] via stochastic simulations and frequency-domain analysis, and identify a dual-site phosphorylation oscillator [29] as the most stable and easily parametrizable.
- 3) **System-level trade-off evaluation:** By comparing a clocked and non-clocked variant and evaluating the effect of decision time on the error probability under RRC constraints, we highlight how timing control can support CRN execution particularly in higher-frequency decision regimes, but that the lower-complexity non-clocked variant can perform better in the low-decision-frequency regime.
- 4) **Adaptive BO scheme for constrained stochastic CRN tuning:** We propose a BO-based optimization approach with adaptive stochastic replication, particularly suited for complex stochastic systems with limited analytical tractability and in line with state-of-the-art methods for experimental chemical reaction optimization. We compare the optimization performance efficiency of the proposed scheme with related optimization schemes and show that it exhibits superior results. Subsequently, we integrate the BO scheme into the ChemSICal-Net framework by targeting communication system objectives.
- 5) **Extension via reuse and scaling:** Lastly, we consider proof-of-concept extensions of the ChemSICal-Net system. We propose a simple reset mechanism and perform

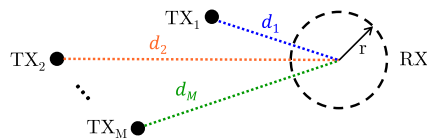


Fig. 3: DBMC scenario with M point TXs at distances $d_1, d_2 \dots d_M$ from a spherical RX.

a preliminary evaluation of its effectiveness. Further, we outline a general path to adding more TXs to the system and discuss challenges with scalability.

The remainder of this paper is structured as follows: In Section II, the physical channel model, communication system, and idealized SIC algorithm for NOMA are introduced. In Section III, we introduce three common and relevant models for chemical oscillation, present evaluation results and choose the most stable option for our system. Then, Section IV presents the structural design of the ChemSICal-Net framework, including integration of the oscillator, as well as reset and TX scaling, while Section V explains the metrics and simulation methods under which we will conduct the evaluation. In Section VI, we showcase the proposed BO scheme and conduct example evaluations against two benchmark schemes before presenting comprehensive simulation results in Section VII. We compare different variants of the ChemSICal-Net system, and quantify the impact of timing control and optimization on the communication performance. Lastly, Section VIII outlines the conclusions. Detailed parameter tables and chemical reaction definitions are given in the Appendix as supplementary material.

II. SCENARIO AND SYSTEM MODEL

We consider a DBMC network with M point TXs, $\text{TX}_1, \dots, \text{TX}_M$ located at distances $d_1 \leq d_2 \leq \dots \leq d_M$ from a single spherical RX of radius r , as illustrated in Figure 3. The RX is assumed to be a passive observer of the instantaneous number of molecules inside its volume $V_{\text{RX}} = \frac{4}{3}\pi r^3$ over time, forming the received signal $n_{\text{RX}}(t)$. Molecules propagate in an unbounded three-dimensional environment via Brownian motion with diffusion coefficient D , and we adopt the uniform concentration assumption (UCA) in the regime $r < 0.15d_i$ [2] to apply the closed-form impulse response model. The TXs are assumed to be one-dimensional points capable of instantaneously emitting molecules. Thereby, for TX_i emitting N_{TX} molecules at time $t = 0$ and distance d_i from the RX, the average contribution to the received signal over time t is given by [2]

$$\lambda_i(t) = \frac{N_{\text{TX}} V_{\text{RX}}}{(4\pi D t)^{\frac{3}{2}}} \exp\left(-\frac{d_i^2}{4Dt}\right) \text{ for } t \geq 0. \quad (1)$$

A. Communication System

Each TX employs on-off-keying (OOK) to transmit information with equiprobable symbols $s_i \in \{0, 1\}$ by emitting either N_{TX} molecules for a '1' or zero molecules for a '0' at the beginning of each symbol interval. We assume independent molecule behavior and model the received signal contribution from each TX as a Poisson-distributed random variable with mean $\lambda_i(t)$. This assumption is valid for sufficiently large N_{TX} and $\lambda_i(t) \ll N_{\text{TX}}$ [36], conditions which hold for our

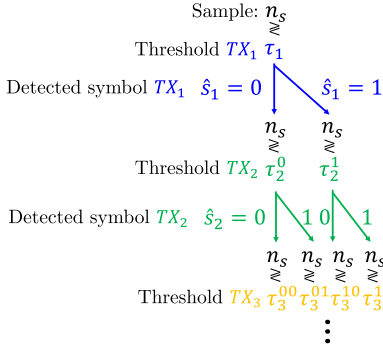


Fig. 4: Simplified threshold-based SIC algorithm for DBMC, adapted from [20].

parameter choices later, see Table I. To keep the chemical evaluation focused on the RX-side, we assume a baseline scenario that is fully synchronized, such that all signals arrive at the RX simultaneously, and we select a sufficiently large symbol period such that inter-symbol interference (ISI) is negligible. We assume peak sampling at the RX, such that each symbol interval is characterized by a single sample. Specifically, the RX takes one sample at the peak time t_p of the received signal as the sampled number of molecules $n_s = n_{RX}(t_p)$, which is the only input used by the subsequent SIC detection algorithm [13]. As defined by the NOMA for DBMC networks (DBMC-NOMA) scheme [8], all TXs transmit simultaneously using the same molecule type. Since the sum of multiple Poisson variables is itself Poisson distributed, the sample n_s follows a Poisson distribution, i.e.

$$n_s \sim \mathcal{P}(\mathbf{s} \cdot \boldsymbol{\lambda}). \quad (2)$$

with the transmitted symbol pattern $\mathbf{s} = [s_1, \dots, s_M] \in \{0, 1\}^M$ and the vector of corresponding received averaged $\boldsymbol{\lambda} = [\lambda_1, \dots, \lambda_M]$. For the general multi-user case with M TXs and equiprobable OOK symbols, the induced distribution over n_s can be expressed as a mixture of 2^M Poisson components, resulting in

$$p_{n_s}[n] = \frac{1}{2^M} \sum_{\mathbf{s} \in \{0, 1\}^M} \mathcal{P}_{\text{PMF}}(n; \mathbf{s} \cdot \boldsymbol{\lambda}), \quad (3)$$

where $\mathcal{P}_{\text{PMF}}(n; \boldsymbol{\lambda}) = \lambda^n \frac{e^{-\lambda}}{n!}$ denotes the probability mass function (PMF) of a Poisson distribution evaluated at n with mean λ . For example, for the two-user baseline ($K = 2$) utilized through most of the paper, the induced distribution over n_s is a mixture of 4 Poisson components with peaks at $n = 0$, λ_1 , λ_2 , and $\lambda_1 + \lambda_2$, respectively.

B. NOMA and Successive Interference Cancellation

By utilizing NOMA, TXs transmit simultaneously and with the same molecule type. To deal with the resulting multiple-access interference (MAI), successive interference cancellation (SIC) is employed as the RX-side algorithm that separates the transmitted symbols and assigns them to each TX based on differences in the expected received amplitude [8], for example due to differing distances d_i . In the case of single-sample peak detection, SIC can be described as a binary-tree threshold procedure, as depicted in Figure 4, where the same n_s is compared multiple times with a threshold set that depends

on previously detected symbols [20]. We opt for this SIC description for clarity and extensibility. In the two-user case ($K = 2$), SIC uses a first-stage threshold τ_1 to detect the symbol \hat{s}_1 for TX₁, and then selects $\tau_2^{\hat{s}_1} \in \{\tau_2^0, \tau_2^1\}$ for TX₂ detection. For $K > 2$, the threshold set generalizes to $\tau_i^{\hat{s}_{i-1}}$ with $\hat{s}_{i-1} = [\hat{s}_1, \dots, \hat{s}_{i-1}]$, yielding a full binary decision tree with 2^{i-1} thresholds at stage i . The detection procedure for a given threshold produces the detected symbol \hat{s}_i with

$$\hat{s}_i = \begin{cases} 1 & n_s \geq \tau_i^{\hat{s}_{i-1}}, \\ 0 & \text{otherwise.} \end{cases} \quad (4)$$

For more details, we refer to our prior work, which provides an analytical error probability derivation for DBMC-NOMA as well as optimization protocols [8], [37].

III. COMPARISON OF CHEMICAL OSCILLATORS

A key limitation of the baseline ChemSICAL design, as discussed in Section I, is that all reactions execute simultaneously and correct SIC behavior depends on the relative differences in RRCs resulting in an implicit reaction results ordering. Faster reactions produce results, which can still influence the slower reactions. The assumption of concurrent reactions is generally valid, as future IoBNT nodes might only consist of a single synthetic cell acting as a reaction volume [5]. However, in ChemSICAL-Net, we introduce an explicit chemical clock to provide controlled time windows in which subsets of the reaction blocks are executed. The goal of this extension is to enable explicit speed-accuracy tradeoffs and avoid relying on high-precision RRC separation across multiple orders of magnitude. On the other hand, adding an oscillating circuit will add complexity and noisy variations to the system, which could impact the stochastic performance negatively. To control reaction blocks using a chemical clock, an oscillating species is incorporated into the associated reactions, so that corresponding reactions are gated by the presence of this oscillating species. Reaction blocks can then be ordered by choosing complementary non-overlapping oscillating species and using them to control subsequent reaction block steps [9]. For this to work reliably, the frequency and amplitude of the oscillating species need to be stable across many oscillation periods.

In this section, we describe and evaluate a set of candidate oscillators as timing sources. We choose three representative models for detailed analysis using a Monte Carlo simulation (MCS) approach with repeated stochastic simulations and a frequency-domain stability analysis. The simulations are conducted using the Gillespy2 package in Python [38]. The chosen models cover a range of structural mechanisms and biological origins and offer simple parametrization. For each oscillator, we generate 500 trajectories over a fixed observation window of $T_{\text{obs}} = 2000$ with 4001 sampling points. T_{obs} is given in normalized time relative to the RRCs. The observation time ensures a stable frequency estimation during the fast Fourier transform processing of $\Delta f = 1/T_{\text{obs}} = 5 \cdot 10^{-4}$. This allows us to precisely determine the fundamental frequency f_1 and its amplitude H_1 and their statistical distributions. The parameters of each model are tuned to produce a target fundamental frequency of $f_1 = 0.1$, corresponding to about 200 oscillation periods per trajectory and a total of 10^5 oscillation periods

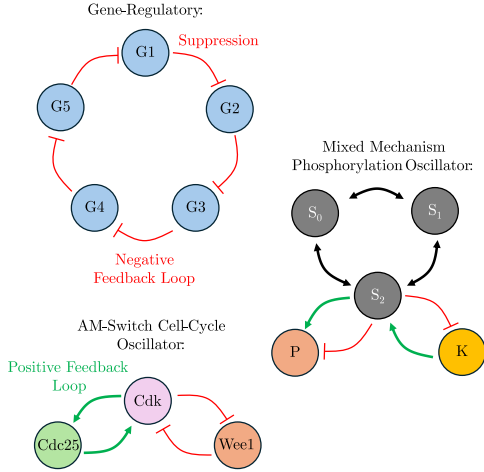


Fig. 5: Simplified structural diagram of the gene-regulatory *Pentilator*, the cell-cycle-based approximate majority (AM) switch oscillator, and a mixed mechanism phosphorylation oscillator. Circles represent molecules/genes, arrows represent relationships such as repression and amplification.

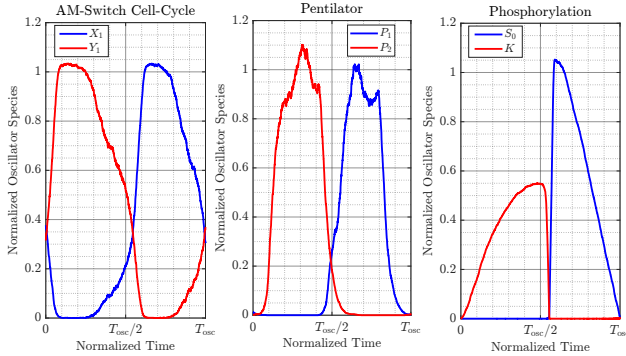


Fig. 6: Example trajectories of three different oscillators over one normalized oscillation period.

per model. Additionally, the peak number of molecules of the oscillating species is also tuned to be approximately 2000 for all models.

A. AM Cell-Cycle Switch Oscillator

The first candidate is a coupled *2-AM Switch* oscillator that is based on a cell-cycle-like structure and the common approximate majority (AM) algorithm [27]. Cell division must be controlled and executed at regular intervals with high reliability. The regulatory mechanism in biological system acts as a switch based on two positive feedback loops (PFBLs), where an activator and inhibitor enzyme interact with each other [39]. The structure of the cell cycle switch is shown in Figure 5. Expressing its fundamental behavior, the cell cycle switch can be reduced to the AM decision algorithm from CRN computing, which from two inputs converts all molecules to the species which was initially in the majority. Coupling two AM switches with negative feedback loops (NFBLs) has been shown to produce sustained oscillations [27]. The model is parametrized mainly by an internal RRC κ_i and an external coupling RRC κ_e and oscillations are obtained for relatively small coupling compared to the internal speed [27]. In this case, we set $\frac{\kappa_e}{\kappa_i} = 0.2$. The full set of reactions and parameters used can be found in the supplementary material. Figure 6

depicts one example period of the *2-AM switch* oscillator on the left side. The selected complementary species X_1 and Y_1 correspond to the activator and inhibitor species of one of the AM switches.

B. Pentilator

The second candidate is the gene-regulatory *Pentilator*, a five-gene variant of the basic *Repressilator* oscillation model. A gene-regulatory oscillator consists of a sequence of genes and proteins, where the protein product of each gene acts as a repressor for the next gene in the cycle forming an NFBL [28]. The *Repressilator* was the first artificially constructed biological oscillating network within living cells [40]. The transcription process is most commonly modeled explicitly using Hill-type propensity functions, i.e. variable RRCs, where each gene transcription reaction has a reaction "speed" of the form

$$f = \frac{\alpha}{1 + P^n}, \quad (5)$$

with the repressor protein P being the preceding protein in the cycle, a scaling parameter α , and the Hill coefficient n . In addition, the oscillator is parametrized by a production rate β of the proteins from mRNA, as well as an mRNA degradation rate d , which can be used to modulate the frequency. The five-gene *Pentilator* variant has been shown to exhibit reduced amplitude and frequency variability [28], which is why we choose it here. A simplified structural diagram of the cycle from gene $G1$ to $G5$ can be seen in Figure 5. For the evaluation, we set $\alpha = 1000$ and the Hill coefficient to $n = 2$. The full model and parameters can be found in the supplementary material. For the time-domain example period in Figure 6, two representative protein trajectories with minimal overlap are chosen.

C. Mixed-Mechanism Phosphorylation

As a third candidate we choose an enzyme-mediated dual-site phosphorylation network, which is derived from natural processes that involve switching complexes such as enzymes and proteins from active to inactive states [27], [29]. Phosphorylation networks describe a process in which a substrate is modified by two counteracting enzymes: a kinase and a phosphatase [29]. The kinase forms the complex by attaching phosphate groups to the substrate site (phosphorylation), while the phosphatase removes them (dephosphorylation). There are different mechanisms of phosphorylation depending on whether the substrate is added and removed individually, or first all are added and then removed. A process combining variants of both is called *mixed-mechanism*. Studies have shown that within specific molecular ratios some mixed-mechanism models are capable of generating oscillations [29], [41]. A simplified diagram of the oscillator is shown in Figure 5. We have selected such an oscillating model from [29], where a parameter configuration with a set of RRCs is suggested, which we have slightly modified for ease of uniform scaling. By scaling the RRCs uniformly the oscillation frequency is modulated. The full parameter set and model can be found in the supplementary material. In Figure 6, we have chosen two species with minimum overlap, which represent the first substrate in the phosphorylation chain S_0 , and the kinase K .

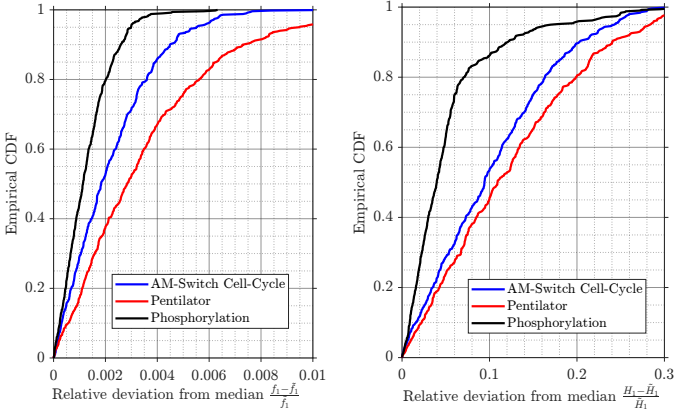


Fig. 7: Empirical CDFs from stochastic simulations of the three considered oscillator models. CDF shows the fraction of trajectories, where the relative deviation from the median fundamental frequency \tilde{f}_1 and fundamental amplitude \tilde{H}_1 is lower than the x -axis value.

D. Evaluation and Selection

Firstly, in Figure 6, we can visually compare the representative trajectories of the three oscillators. While all three exhibit the general desired pattern of oscillating from near-zero to the peak in two molecule species that are offset by half a cycle, there are some notable differences. For example, the Pentilator trajectories seem to showcase a significant amount of noise, while the phosphorylation oscillator appears the most stable. For the latter, we also see the least amount of inter-species overlap, while for the 2-AM and Pentilator variant, there is a significant part of the cycle where both species are present. Secondly, we can take a look at the systematic analysis in Figure 7. Here, we extract the median values of the fundamental frequency and fundamental amplitude, \tilde{f}_1 and \tilde{H}_1 , from the simulated trajectories and plot an empirical cumulative density function (CDF) of the relative deviations $\frac{\tilde{f}_1 - f_1}{f_1}$, $\frac{\tilde{H}_1 - H_1}{H_1}$. In the plot, a line that is further to the top left represents higher stability. The results show the phosphorylation oscillator with the highest stability for both f_1 and H_1 by a significant margin, while the Pentilator exhibits the largest deviations, and the 2-AM oscillator in the middle. Given the two properties of smallest inter-species overlap and highest frequency and amplitude stability, we select the phosphorylation oscillator as the chemical clock we will use for ChemSICAL-Net. We will use the two species shown in Figure 6 to define activation windows for the different SIC stages and evaluate the impact on performance as we will define it in Section V.

IV. CHEMSICAL-NET CRN DESIGN

In this section, we will introduce the baseline ChemSICAL design and its timed extension ChemSICAL-Net, by introducing the chemical block structure underlying the SIC computation, as well as the interface with the phosphorylation oscillator. Additionally, we describe a proof-of-concept reset mechanism and its integration into the system (ChemSICAL-Net+R), and we describe how the structure can be conceptually scaled to many TXs and how the complexity of the system changes (ChemSICAL-Net+TX). The full block diagram of the system design including all extensions can be found in Figure 8. An overview of all the models, the different associated extensions, and their names can be seen in Figure 9.

The objective of ChemSICAL is to implement the SIC detection logic using only chemical reactions. To that end, the observation n_s from the DBMC channel is converted to a chemical representation and processed by a CRN [13]. We represent the sampled input n_s as a discrete molecule count of a designated input species Y_{on} , i.e. $N(Y_{\text{on}}) = n_s$, which can be interpreted as the number of signaling molecules that enter the reaction volume at the RX. An implicit assumption is the existence of a sample-and-hold mechanism, which captures the number of molecules within the RX. This could be addressed in future work, for example, by assuming more complex receptors such as ligand-binding types [1]. The chemical SIC computation then produces two indicator species per TX $_i$ denoted by D_i^0 and D_i^1 in a comparison and decision mechanism which uses the input species Y_{on} and a TX-specific threshold species W_i . For the bit detected via ChemSICAL, we adopt the established decision rule

$$\hat{s}_i^C = \begin{cases} 1 & N(D_i^1) \geq N(D_i^0), \\ 0 & \text{otherwise,} \end{cases} \quad (6)$$

which directly mirrors the binary threshold decisions of the analytical SIC from Section II-B. The CRN is parametrized by numerous additional intermediate species and a set of reaction rate constant (RRC), describing the speed of each reaction. The performance of the chemical RX depends critically on these reaction parameters rather than only on the analytically optimal threshold parameters [13].

The baseline two-stage SIC logic is decomposed into modular reaction blocks that implement comparison, translation, approximate majority (AM), and threshold adaptation. Each TX corresponds to one stage. The second-stage blocks reuse the same constant $N(Y_{\text{on}})$, as it is not consumed, and adapt the threshold for TX $_2$, $N(W_2)$, according to the detection result in stage 1. We make use of the following basic CRN blocks, as defined in [9]:

Comparison: Compares an input species (Y_{on}) to a threshold (W_i) and generates two indicator molecule species ($X_{\text{on},i}$, $X_{\text{off},i}$), the ratio of which indicates the ratio between input and threshold.

Translation: Generates detection species (D_i^0 , D_i^1) of the exact same number of molecules as one or multiple inputs ($X_{\text{on},i}$, $X_{\text{off},i}$). This is used to decouple subsequent reactions, i.e., limit interference of the previous reaction on the reactants of the following ones.

Approximate Majority (AM): Takes two inputs (D_i^0 , D_i^1) and amplifies the species that was initially in the majority, i.e., turns $N(D_i^j) > N(D_i^k)$ into outputs $N(D_i^j) \gg N(D_i^k)$. As a result, many more of one species, and almost none of the other are left, creating an approximate binary decision.

Threshold Adaptation: Corresponds to an addition CRN, similar to Figure 2. The base threshold species molecule count, $N(W_{2,B})$, and the detection species molecule count $N(D_1^1)$ are added to form the threshold species $N(W_2)$. This links the first stage for detecting the bit from TX $_1$ with the second stage for the bit from TX $_2$. The molecule counts of each species must be tuned such that: $N(W_{2,B}) = \tau_2^0$ and $N(X_{\text{on},1}) + N(X_{\text{off},1}) + N(W_{2,B}) = \tau_2^1$. The latter must hold, since the asymptotic result of the first-stage AM block in case

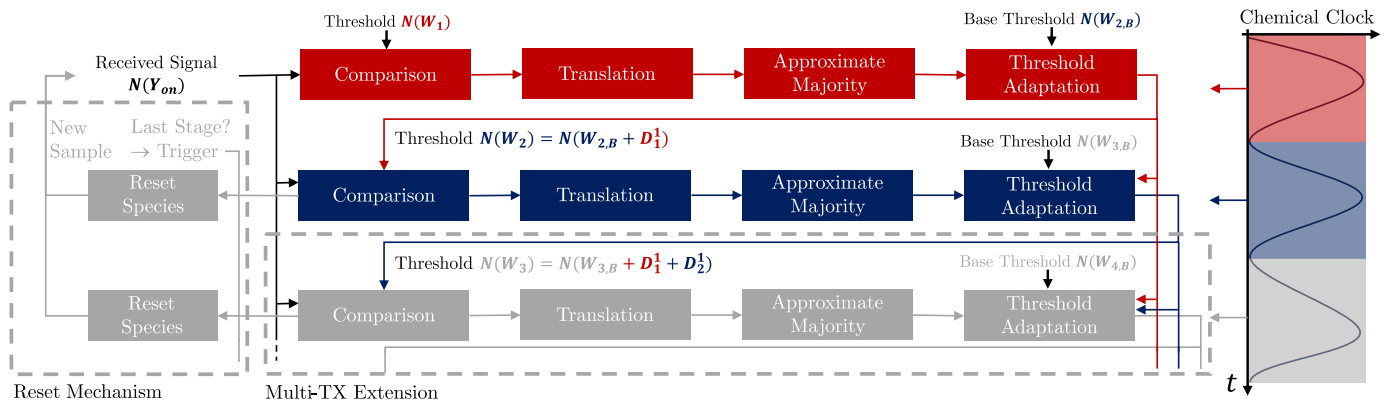


Fig. 8: Proposed ChemSICal-Net block diagram: A CRN implementing a multi-stage SIC algorithm. Stages are controlled by a chemical oscillator. Optional extensions in grey include a reset mechanism and the addition of more TXs.

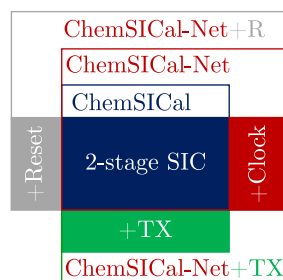


Fig. 9: Compact overview, mirroring Figure 8, of the different model variants utilized throughout the paper and their functional blocks.

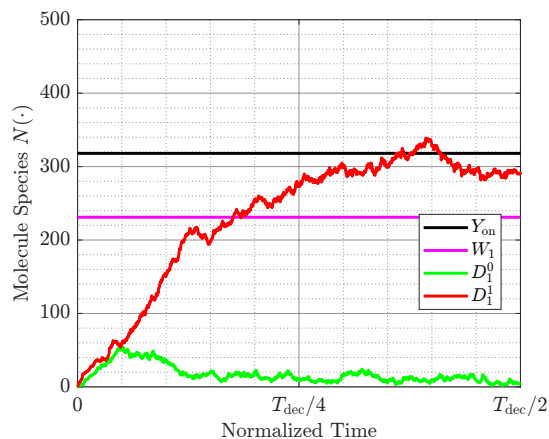


Fig. 10: Example trajectory of the molecule species relevant to the first stage for input $N(Y_{\text{on}}) = 318$, showing the decision variables D_1^0, D_1^1 converging according to the relation between input and threshold (here, $N(Y_{\text{on}}) > N(W_1)$).

of $\hat{S}_1^C = 1$ is $N(D_1^1) \approx N(X_{\text{on},1}) + N(X_{\text{off},1})$.

The full set of chemical reactions per block and for the reset and third TX extension introduced later can be found in the supplementary material.

Each reaction block is parametrized by one RRC that defines the speed of execution of that block. According to each block, we define the RRCs per $\text{TX}_i/\text{stage } i$: $\kappa_{C,i}$ for *Comparison*, $\kappa_{T,i}$ for *Translation*, $\kappa_{AM,i}$ for *AM*, and $\kappa_{TA,i}$ for *Threshold Adaptation*. We maintain the single-volume assumption for the entire CRN, meaning there is no need for separate compartments, but a requirement for correct temporal

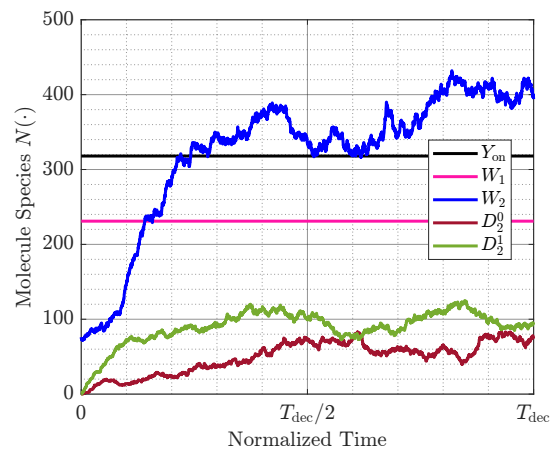


Fig. 11: Example trajectory of the molecule species relevant for the second stage for input $N(Y_{\text{on}}) = 318$, for the configuration *without* timing control, i.e. all stages are running simultaneously. The plot shows the molecule counts of D_2^0, D_2^1 converging *incorrectly* since the threshold $N(W_2)$ needs to be adapted in reaction to the first-stage detection, but the second stage already starts computing based on the wrong value of $N(W_2)$.

ordering via chemical design. In the baseline ChemSICal model [13], the ordering must be implicitly achieved by tuning the RRCs across stages so that stage-2 computations take place after stage-1 computations have finished. Figure 10 shows an example trajectory for the input $Y_{\text{on}} = 318$, we can see how the species for Y and W_1 remain constant and the decision variables react in response to the input, showing D_1^1 as the clearly larger concentration at the end. In Figure 11, we show the entire SIC cycle until the decision time T_{dec} , for the case of the baseline ChemSICal where both stages run simultaneously. The parameters for this case are optimized using the scheme later presented in Section VI. We can see that the second symbol is actually incorrectly detected. The threshold $N(W_2)$ is adapted, i.e. increased, since we detect a '1' for TX_1 . Initially $N(Y_{\text{on}}) > N(W_2)$, and the second stage starts to produce more D_2^1 molecules (see dark green line). However, the adaptation causes $N(W_2)$ to exceed $N(Y_{\text{on}})$ eventually, which means D_2^0 should dominate the detection. However, the second stage ends up in an unstable and undecided state, where $N(D_2^0) \approx N(D_2^1)$. The main reason lies in the fact that the second stage already reacts to the incorrect thresholds at

the very beginning and does not correct itself later, when the threshold has changed. In the next section, we will discuss the extension to explicit ordering using a chemical clock, which can help in this case.

A. Chemical Clock Integration - ChemSICal-Net

The novel model variant ChemSICal-Net (see Figure 9) integrates a chemical oscillator that generates a repeatable phase signal. This phase signal is mapped to SIC stages such that reactions are predominantly active in intended time windows, rather than competing immediately from $t = 0$.

As discussed in Section III, we select the dual-site phosphorylation oscillator, which provides multiple oscillating species with minimal inter-species overlap, e.g., S_0 and the kinase K . To gate stage 2 (blue row in Figure 8), we multiply the propensity function of each reaction block in that stage by a common Hill activation factor based on S_0 ,

$$g_{S_0}(t) = \frac{N(S_0)(t)^{n_{S_0}}}{N(S_0)(t)^{n_{S_0}} + S_{0,\text{half}}^{n_{S_0}}}, \quad (7)$$

with Hill coefficient n_{S_0} and half-activation value $S_{0,\text{half}}$, which jointly determine the steepness of the clock-induced activation transition. Similarly, we can define a Hill activation factor $g_K(t)$ based on the kinase K .

We illustrate the timing effect in Figure 12 using the same input and species selection as in Figure 11. Here, we define the *decision horizon* T_{dec} as the time at which the CRN output is read out (see Section V-B). For timed variants, we tune the oscillator such that one full period equals the decision horizon, i.e., $T_{\text{osc}} = T_{\text{dec}}$. Consequently, for the two-stage case, stage 2 is activated predominantly during the second half-cycle, starting at $T_{\text{osc}}/2 = T_{\text{dec}}/2$. The shown trajectory yields a correct final decision and highlights how the threshold W_2 is first adapted based on detection stage 1 (see Figure 10) before the second stage is enabled.

Overall, ChemSICal-Net provides a tunable decision time per symbol by adjusting T_{dec} (and thus T_{osc} in timed variants): smaller T_{dec} increases throughput but risks incomplete reaction processing, whereas larger T_{dec} improves CRN reliability at the cost of latency.

B. Further Extensions

1) Additional TXs

The ChemSICal-Net block structure can be extended beyond two TXs by repeating the stage pattern consisting of *Comparison*, *Translation*, and *AM* for each additional TX and by introducing an additional *Threshold Adaptation* step per added stage. For a third TX (TX₃), we introduce a third stage with threshold species W_3 and decision species D_3^0 and D_3^1 , and the corresponding computation blocks are indicated by the shaded *Multi-TX Extension* region in Figure 8. The key additional operation is the formation of the stage-3 threshold W_3 from a base threshold $W_{3,B}$ and the detection evidence produced by the prior stages, where the conceptual structure in Figure 8 corresponds to an additive update of the form $N(W_3) = N(W_{3,B}) + N(D_1^1) + N(D_2^1)$. The molecule counts of $W_{3,B}$ and the effective contribution of the decision evidence are tuned such that the resulting chemical thresholds match the intended analytical SIC thresholds along the relevant decision

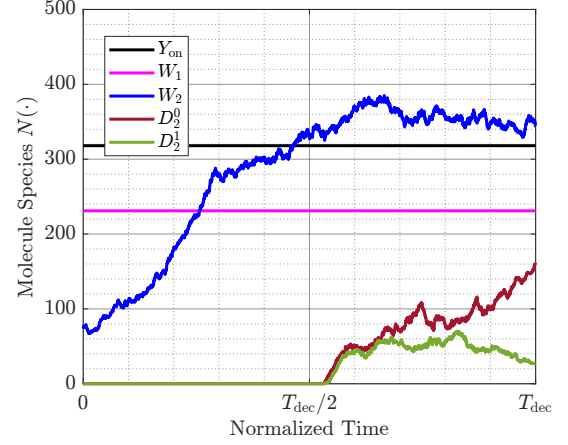


Fig. 12: Example trajectory of the molecule species relevant for the second stage for input $N(Y_{\text{on}}) = 318$, for the configuration *with* timing control. The plot shows the decision variable molecule counts of D_2^0, D_2^1 are converging *correctly* (in contrast to Figure 11), since the threshold $N(W_2)$ can be adapted in the first half of the decision time, and the second-stage reactions start computing only in the second half based on correct input values.

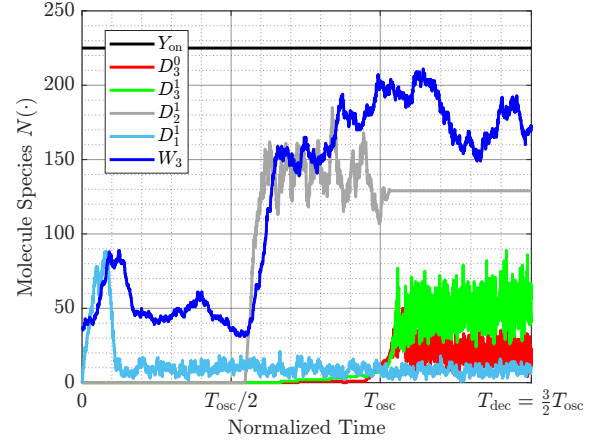


Fig. 13: Example trajectory of the molecule species relevant for the third stage for an input of $N(Y_{\text{on}}) = 225$. The plot shows the threshold $N(W_3)$ is adapted based on the decision species for stage 1 (light blue) and stage 2 (grey) and ultimately leads to the correct decision for stage 3, since $N(Y_{\text{on}}) > N(W_3)$.

branches. To prevent premature computation with a non-adapted threshold, the stage-3 reaction blocks are activated in a dedicated time window after stage 1 and stage 2 have completed their threshold adaptation and decision formation. In the example structure in Figure 8, the stage-2 and stage-3 blocks are controlled by different clock phases so that the three stages are executed sequentially, each within one oscillation period without overlap.

In terms of complexity growth, for M TXs, ChemSICal-Net comprises M copies of the *Comparison*, *Translation*, *AM* blocks plus $M - 1$ *Threshold Adaptation* blocks, i.e., $B(M) = 3M + (M - 1) = 4M - 1$ logical blocks and thus reactions/species scale linearly with M . However, for threshold formation, stage i aggregates the base threshold and the prior decision evidence,

$$N(W_i) = N(W_{i,B}) + \sum_{j=1}^{i-1} N(D_j^1), \quad (8)$$

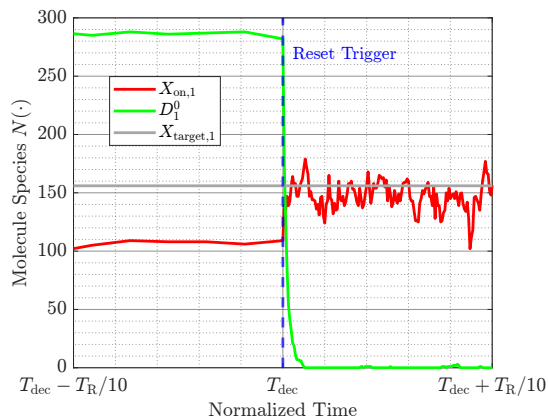


Fig. 14: Example trajectory of the molecule species relevant for the reset mechanism. We show a small snippet just before and just after the reset trigger. We show a selected decision species D_1^0 returning to a molecule count of zero, and the intermediate comparison species molecule count $N(X_{\text{on},1})$ being reset to its target value within a short amount of time.

so adding one TX increases the threshold adaptation by one additional evidence term per subsequent stage, which leads to polynomial growth. The exponential growth that is usually associated with a binary tree decision mechanism (see SIC structure in Figure 4) can be avoided, due to the design of ChemSICal-Net as a successive aggregator of bit decisions for threshold adaptation. We treat the 3-TX variant as a proof-of-concept extension to demonstrate feasibility and scaling trends, and we restrict the detailed optimization study to a representative configuration. Figure 13 illustrates an example trajectory excerpt, highlighting two consecutive threshold-adaptation steps and the delayed activation of the third-stage decision dynamics.

2) Reset Mechanism

The baseline ChemSICal and ChemSICal-Net models are one-shot computations, because internal intermediates and the AM outputs accumulate over time and settle into strongly imbalanced states that cannot be reused without reinitialization. ChemSICal-Net+R introduces an explicit reset phase that restores selected internal species to well-defined initial conditions at the end of each symbol period, enabling repeated symbol processing with the same reaction volume. We distinguish two reset actions, namely clearing species that should return to zero (e.g., decision and intermediate species) and restoring species that should return to fixed reference values. The reset is controlled by a dedicated trigger species that activates reset reactions only during a designated reset window, as indicated by the dashed *Reset Mechanism* block in Figure 8. This trigger is not explicitly modeled for this proof-of-concept evaluation but it could be connected to an appropriate oscillation species similar to the chemical clock with a slower frequency to activate only after all stages have been computed. For clearing, the trigger activates reactions that convert targeted species into inert waste products, which effectively removes residual molecules without altering the held input Y_{on} during the decision phase. For restoration to reference values, the trigger activates reactions that release reference molecules from protected reservoir species into the active pool, thereby recreating the desired initial molecule

counts without requiring external injection of each individual species. In the timed design, the reset window is scheduled after all detection stages have completed, so that reset reactions do not interfere with threshold adaptation or decision formation. Figure 14 illustrates an excerpt of an example reset cycle in which, D_1^0 , a decision-related species is driven back to zero and, $X_{\text{on},1}$, a reference species is restored to its target molecule count before the subsequent computation begins. The overall reset cycle lasts for time T_R .

V. SIMULATION SETUP

In this section, we define the performance metrics used to evaluate our system, describe the solvers and stochastic simulation algorithms (SSAs) used to simulate the CRN, and outline the MCS evaluation structure.

A. Solvers and Simulation Methods

The evaluation metrics are based on the chemical detection outcomes \hat{s}_i^C and therefore on the terminal molecule counts of the detection species pairs (D_i^0, D_i^1) as defined in the system model. The correctness of the CRN outcome depends on the input value $N(Y_{\text{on}})$, i.e., on the sampled received signal n_s , which dictates the expected outcome according to the non-chemical SIC decision rule. We evaluate the CRN using both a deterministic solver and a stochastic solver, because the deterministic mean-field behavior alone does not capture the probabilistic dynamics that emerge at finite molecule counts. The deterministic solver converts the CRN into a set of ODEs and computes continuous time-varying concentration trajectories for all species, which is useful for qualitative validation and debugging of reaction ordering. The stochastic solver applies an SSA based on Gillespie’s algorithm, which generates statistically accurate sample trajectories of the discrete-state CRN dynamics. In each SSA trajectory, intrinsic molecular noise is reflected by random reaction event times driven by stochastic molecule interactions, and repeated trajectories are therefore required to characterize detection performance statistically. Additive external molecular noise sources such as leakage molecules are not modeled in the present setup, and their inclusion is expected to primarily shift effective thresholds and error regions rather than alter the qualitative operation.

B. Performance Metrics

For a given input molecule count $N(Y_{\text{on}})$, we define a binary correct-detection indicator as $c[N(Y_{\text{on}})] \in \{0, 1\}$ for deterministic evaluation and as $c_j[N(Y_{\text{on}})] \in \{0, 1\}$ for a single SSA trajectory j . A trajectory is considered correct if the CRN returns the correct joint decision $[\hat{s}_1^C \hat{s}_2^C]$ for the given input $N(Y_{\text{on}})$, where each \hat{s}_i^C is obtained by comparing the terminal counts of (D_i^0, D_i^1) according to the decision rule (6) in the system model. For reset-enabled variants, the per-trajectory correctness check additionally requires that designated species are returned to their intended post-run target state within a tolerance band, so that correct decisions are only counted if the run is both correct and reusable. The probability of correct detection for a given input and N_{traj}

TABLE I: Communication System Parameters

Parameter	Symbol	Values
Number of TXs	M	2, 3
TX distances	$\{d_1, d_2, d_3\}$	$\{10, 12, 14\}$ μm
RX radius	r	1 μm
Diffusion coefficient	D	1×10^{-9} $\text{m}^2 \text{s}^{-1}$
Molecules sent per bit-1	N_{TX}	1×10^6 molecules
SIC thresholds ($K = 2$)	$\{\tau_1, \{\tau_2^0, \tau_2^1\}\}$	$\{231, \{78, 386\}\}$ molecules
SIC thresholds ($K = 3$)	$\{\tau_1, \{\tau_2^0, \tau_2^1\}, \{\tau_3^{00}, \tau_3^{01}, \tau_3^{10}, \tau_3^{11}\}\}$	$\{267, \{114, 422\}, \{35, 192, 343, 500\}\}$ molecules

TABLE II: CRN Initial Values

Parameter	Symbol	Initial Value (before BO)
Input Species	Y_{on}	$0 \leq N(Y_{\text{on}}) \leq 600$ molecules
Comparison Species	$\{X_{\text{on},1}, X_{\text{off},1}\}$	154, 154 molecules
	$\{X_{\text{on},2}, X_{\text{off},2}\}$	83, 84 molecules
	$\{X_{\text{on},3}, X_{\text{off},3}\}$	35, 36 molecules
Detection Species	$\{D_i^0, D_i^1, i \in \{1, 2, 3\}\}$	$\{0,0,0\}$ molecules
Threshold Species	W_1	231 molecules
	$\{W_{2,B}, W_2\}$	78, 78 molecules
	$\{W_{3,B}, W_3\}$	35, 35 molecules
Helper Species	$\{B_1, B_2, B_3\}$	$\{0,0,0\}$ molecules

TABLE III: CRN Kinetic Parameters

Parameter	Symbol	Value
ChemSICal-Net RRCs	$\kappa_{C,i}, \kappa_{\text{Tr},i}, \kappa_{\text{AM},i}$	Before BO: see Table V
	$\kappa_{\text{TA},i}, i \in \{1, 2, 3\}$	After BO: see Suppl. Mat.
Rate bounds	$\{\kappa_{\text{min}}, \kappa_{\text{max}}\}$	$\{10^{-3}, 1\}$
Oscillator rates	$\kappa_1, \dots, \kappa_{10}$	see Suppl. Mat.
Time reference	T_{ref}	73 [unit-less]
Oscillation period	T_{osc}	$\{T_{\text{ref}}/4, T_{\text{ref}}/2, T_{\text{ref}}, 2T_{\text{ref}}\}$
Reset rates	$\kappa_{\text{clear}}, \kappa_{\text{copy}}, \kappa_{R,\text{decay}}$	see Suppl. Mat.
Hill half-activation K	K_{half}	600 molecules
Hill half-activation S_0	$S_{0,\text{half}}$	600 molecules
Hill coefficients	n_K, n_{S_0}	$\{1, 1\}$

different trajectories j is estimated as

$$P_d[N(Y_{\text{on}})] = \frac{1}{N_{\text{traj}}} \sum_{j=1}^{N_{\text{traj}}} c_j [N(Y_{\text{on}})]. \quad (9)$$

The primary aggregate metric is an input-weighted probability of error, where errors are weighted by the input PMF $p_{n_s}[N(Y_{\text{on}})]$ such that unlikely inputs have less influence than likely ones. We compute the input-weighted error probability as

$$P_e = 1 - \sum_{N(Y_{\text{on}})} p_{n_s}[N(Y_{\text{on}})] \cdot P_d[N(Y_{\text{on}})], \quad (10)$$

which is equivalent to weighting the correct-detection probability and converting to an error metric. We additionally define a reduced input-weighted error probability by restricting the sum to a selected subset of input values that capture the high-likelihood region of the input distribution, which yields a more efficient objective for parameter search. We define the decision time T_{dec} , i.e., the time at which CRN states are read out and mapped to $[\hat{s}_1^C, \hat{s}_2^C]$, and T_{dec} is treated as a key design knob in the evaluation.

C. Monte-Carlo Simulations

For each parameter configuration and each evaluated input molecule count $N(Y_{\text{on}})$, we generate N_{traj} independent SSA trajectories up to the decision time T_{dec} and compute $P_d[N(Y_{\text{on}})]$ as an empirical mean of correctness outcomes. The overall input-weighted metric is obtained by combining the per-input estimates using the weights given by the input PMF from the communication system model. We report a 95% confidence interval (CI) for Monte-Carlo estimates using a normal approximation for proportions with a z -multiplier of 1.96,

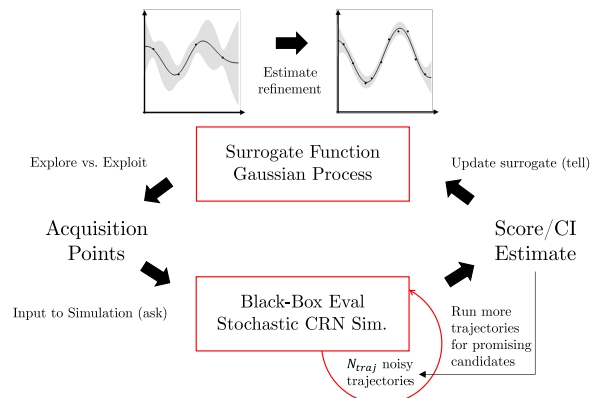


Fig. 15: Illustration of the BO loop, where noisy black-box evaluations are used to update a surrogate model, and an acquisition rule balances exploration and exploitation to select the next candidates.

and we use the corresponding CI half-width as an indicator of estimation reliability. Unless stated otherwise, full evaluations use a high trajectory count per input to obtain stable P_d curves and reliable weighted error estimates, whereas optimization loops may use smaller budgets and increase N_{traj} only for promising or uncertain configurations.

VI. OPTIMIZATION SCHEME COMPARISON AND SELECTION

We treat the ChemSICal-Net system as a black-box optimization problem over a bounded parameter space because the objective is stochastic, non-convex, and only available as an estimate obtained from multiple SSA runs. Our goal is to minimize the likelihood-weighted error probability P_e , where correctness is estimated per input Y_{on} from Monte-Carlo trajectories and then weighted by the input likelihood as defined in Section II. Equivalently, we maximize the detection accuracy $1 - P_e$.

The optimization variables consist of the set of RRCs of the reaction blocks, denoted by \mathcal{K} , as well as the initial molecule species concentrations, denoted by \mathcal{N} . This yields the constrained optimization problem

$$\begin{aligned} & \underset{\mathcal{K}, \mathcal{N}}{\text{minimize}} && P_e(\mathcal{K}, \mathcal{N}) \\ & \text{subject to} && \kappa_{\text{min}} \leq \kappa_i \leq \kappa_{\text{max}}, \quad \kappa_i \in \mathcal{K}, \\ & && N_j \in \mathbb{Z}_{\geq 0}, \quad N_j \in \mathcal{N}. \end{aligned} \quad (11)$$

To solve this problem, we propose an adaptive BO scheme as the default optimizer. To evaluate its effectiveness against other state-of-the-art black-box methods, we additionally consider SA and a MH-MCMC scheme, and we compare all methods under matched evaluation settings in a small set of representative scenarios.

A. Baseline Optimization Setup

To reduce computational effort, we do not optimize over a dense sweep of possible Y_{on} values. Instead, we evaluate candidates on a sub-sampled input vector that is chosen to cover both (i) regions with high input likelihood and (ii) regions close to the relevant decision thresholds, where errors are most likely to occur. This sub-sampling reduces the number of inputs per objective evaluation significantly, while still capturing the dominant contribution to the likelihood-weighted objective.

Since the objective is noisy due to finite Monte-Carlo sampling, each candidate must be evaluated using multiple SSA trajectories. To improve sample efficiency, we apply an adaptive replication scheme in which candidates are evaluated in successive rungs with increasing numbers of trajectories per input. In our setup, we use the rung schedule [20, 60, 100, 500] trajectories per input, such that the first rung enables fast screening and later rungs provide high-confidence evaluation for candidates that appear competitive. A candidate is promoted to the next rung if it either reaches a rung-specific performance threshold ($1 - P_e \geq 0.90, 0.95, \text{ and } 0.99$ for successive rungs) or if its estimated uncertainty remains large (CI half-width of $1 - P_e > 0.1$), which prevents discarding candidates that might be strong but insufficiently sampled.

To enable a fair complexity comparison across optimization schemes, we report optimization performance against the cumulative number of simulated SSA trajectories required to reach a given score, rather than against iteration count alone. This is particularly important because adaptive replication makes the evaluation cost candidate-dependent.

B. Adaptive Bayesian Optimization Scheme

Our BO scheme follows an ask-tell loop with a Gaussian process surrogate model and an expected-improvement (EI) acquisition function. The surrogate provides both a predicted objective value and an uncertainty estimate for each point in the parameter space, and the EI acquisition balances exploration of uncertain regions with exploitation of regions that are predicted to perform well. We use a Matérn kernel for the surrogate.

We evaluate candidates in batches to leverage parallel computation, while feeding all completed evaluations back into the surrogate model. The resulting structure is summarized in Figure 15, where the black-box objective evaluations update the surrogate, and the acquisition mechanism determines the next candidate parameters.

C. Comparison with Benchmark Schemes

1) Simulated Annealing

We implement simulated annealing [34] as a multi-chain scheme to exploit parallelism and reduce sensitivity to initialization. The method uses a temperature schedule that cools over the number of batch steps, enabling broader exploration early in the run and more local refinement later. We replicate the settings employed for CRN optimization using SA in related work [35]. Candidate proposals are generated as Gaussian steps in \log_{10} space for log-scaled rate parameters, which corresponds to multiplicative perturbations in the original parameter domain. The proposal step sizes are adapted

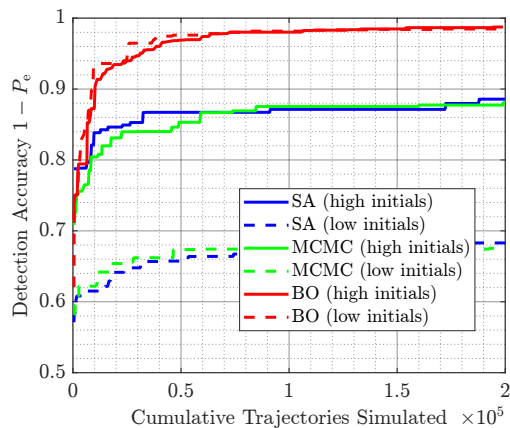


Fig. 16: Comparison of optimization schemes showing achieved score versus the cumulative number of simulated SSA trajectories on the x -axis for BO, SA, and MCMC, using high- and low-value initializations for the RRCs. Results are shown as an average across 3 independent optimization runs per scheme.

periodically to target an acceptance rate of approximately 0.3, which reduces wasted evaluations from near-certain rejection while maintaining sufficient exploration.

To ensure a like-for-like comparison with BO, SA uses the exact same adaptive replication evaluator described in Section VI-A, including the same rung schedule and the same uncertainty-aware promotion rule.

2) MCMC with Metropolis-Hastings Method

We implement an MCMC-style optimizer based on a Metropolis-Hastings acceptance rule, using multiple parallel chains and random-scan proposals that update one parameter at a time. This design is computationally stable in our setting because each objective evaluation is expensive and the acceptance decision can be made using only the scalar objective estimate.

The acceptance ratio uses the same scaling as Murphy et al. in related work [32], which treats the score as a probability-like quantity and calibrates acceptance such that a 1% decrease in score is accepted with probability 0.25. This scaling prevents overly greedy behavior when scores are close to one, while still biasing the search toward high-performing regions. The proposal scales are adapted periodically to target an acceptance ratio around 0.25, which avoids collapse into extremely small steps and reduces wasted evaluations on near-certain rejections.

As for SA, the MCMC benchmark uses the same adaptive replication evaluator as BO and therefore differs only in the search policy and acceptance mechanism.

D. Benchmark Scenarios and Selection Outcome

We compare BO, SA, and MCMC on representative ChemSICal-Net optimization scenarios, focusing on a fixed processing horizon $T = T_{\text{ref}}$. To incorporate sensitivity to initialization, each scheme is run from two different starting configurations of the RRCs, namely a high initialization where all RRCs start near the upper bound and a low initialization where all RRCs start near the lower bound. For each initialization, three independent optimization runs per scheme are generated.

TABLE IV: Simulation and Optimization Parameters

Parameter	Symbol	Value
Trajectories per input	N_{traj}	Standard: 200 Optimization Rungs: [20, 60, 100, 500]
Optimization rung thresholds	$(1 - P_e)_{\text{th}}$	[0.9, 0.95, 0.99]
Confidence interval	z	$z = 1.96$ for 95% CI (proportions)
Time reference	T_{ref}	73 [unit-less]
Decision time horizon	T_{dec}	$\{T_{\text{ref}}/4, T_{\text{ref}}/2, T_{\text{ref}}, 2T_{\text{ref}}\}$
Input set for evaluation	$Y_{\text{on}} \in \mathcal{Y}$	Standard: $\mathcal{Y} = \{0, 1, \dots, 600\}$ Optimization (2-TX): $\mathcal{Y} = \{140, 167, 216, 308, 400, 475\}$ Optimization (3-TX): $\mathcal{Y} = \{71, 157, 228, 308, 379, 465, 536\}$
Optimization iterations	N_{iter}	1000

TABLE V: Reaction constant sets utilized in Figure 17.

Set	$\kappa_{C,1}$	$\kappa_{Tr,1}$	$\kappa_{AM,1}$	$\kappa_{TA,1}$	$\kappa_{C,2}$	$\kappa_{Tr,2}$	$\kappa_{AM,2}$
1	1.0	1.0	1.0	1.0	1.0	1.0	1.0
2	1.0	1.0	1.0	1.0	0.1	0.1	0.1
3	1.0	1.0	0.1	1.0	0.1	0.1	0.01
4	1.0	1.0	0.1	1.0	0.1	0.01	0.001
5	1.0	1.0	0.1	1.0	0.1	0.1	0.001

We summarize the achieved best-so-far score as a function of the cumulative number of simulated trajectories, which provides a fair comparison in terms of computational complexity and resource usage. Figure 16 shows that BO achieves higher scores than both benchmarks for the same simulation budget, reaching accuracies above $1 - P_e = 0.95$ within approximately 2×10^5 trajectories and showing consistent performance under both initializations. In contrast, SA and MCMC converge to lower scores < 0.9 and exhibit substantially larger differences between high and low initializations, where the low initialization yields scores < 0.7 .

Based on these results, we select adaptive BO as the default optimization scheme for the remainder of the paper because it provides the strongest sample efficiency and the most robust convergence behavior across the tested initializations.

VII. EVALUATION OF CHEMSICAL-NET

In the following, we will present a thorough evaluation of the ChemSICAL-Net design. Firstly, we will utilize ODE-based results of the algorithm performance across the possible DBMC channel input range of the Y_{on} molecule species. This will provide a first intuition about the more challenging input regions and show the limitations of the ODE-based tuning approach, as it leaves a large error probability in the stochastic simulations, see Section V. Then, we systematically apply our BO framework to evaluate the stochastic simulation results of the ChemSICAL-Net system and optimize the RRCs and initial molecule concentrations. We compare different variants of ChemSICAL, highlighting the impact of timing control and the BO scheme on the error probability P_e . The system with timing control through the chemical oscillator will be denoted as ChemSICAL-Net or *Timed*, while the system without timing control is denoted as *Always-On* or *AO*. Lastly, we present initial evaluations of our concepts for ChemSICAL-Net+R, for the reset mechanism, and ChemSICAL-Net+TX, for adding another TX to the system. The most important parameters utilized for the communication system, the ChemSICAL-Net initial molecule counts and RRCs, and the BO scheme can be found in Tables I, II, III, and IV. Any specific additional parameter values are listed in the supplementary material.

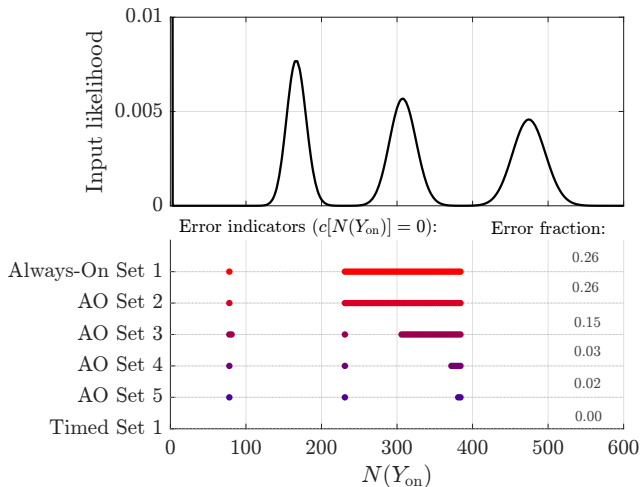


Fig. 17: Results of the ODE-based evaluation across different RRC sets (shown in Table V) for the *Always-On* (AO) and the *Timed* variant of the ChemSICAL-Net system. The markers show occurrences of errors within the range of inputs $N(Y_{\text{on}})$ and the input likelihood is shown on top in black.

A. Initial ODE Tuning

As we identified in prior work [13], the RRCs are the most important factor in determining the correct operation of the ChemSICAL-Net algorithm. Therefore, we will firstly use the fast ODE solver to generate an overview of the effect of different sets of RRCs, as defined in Table V, for both the *Timed* and *Always-On* variant and for a decision time horizon of $T_{\text{dec}} = T_{\text{ref}}$. With the ODE solver, each input value of $N(Y_{\text{on}})$ causes a result that is either correct or incorrect. In Figure 17, the errors ($c[N(Y_{\text{on}})] = 0$) are indicated in relation to the value of $N(Y_{\text{on}})$ and the input likelihood distribution $p_{\text{ns}}[Y_{\text{on}}]$. For set 1, all RRCs are set equal to $\kappa_{\text{max}} = 1$. For the *Always-On* variant, we see a significant number of errors across a large range of input values including ones with high likelihood. This is related to the problem of operation ordering. Since all reactions happen at the same time, if they are also happening at the same speed, later steps in the system are not being computed based on the correct results from prior steps. We show an example of such an issue in Section IV, Figure 11. The progression of RRC sets 1 to 5 was chosen by hand to showcase how to mitigate this problem in the *Always-On* case. Sets 2 and 3 show that it is not enough to make all reactions of stage-2 slower, or further slowing down the AM reactions by an order of magnitude, although set 3 has a slightly reduced error fraction and we are directionally correct with these changes. Lastly, set 4 and 5 suggest that the AM reaction for stage-2 must be slower by around three orders of magnitude,

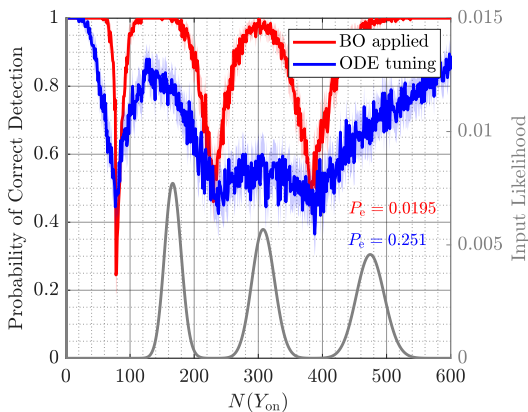


Fig. 18: Comparison of the detection accuracy $P_d[N(Y_{\text{on}})]$ over the input range of the molecule species Y_{on} between the ODE-tuned parameters in blue and the BO-optimized parameters in red. Input likelihood of $N(Y_{\text{on}})$ for reference in grey. Input-weighted error probability of the entire system P_e also shown. *BO improves P_d a lot in high-likelihood regimes; P_e is reduced from 0.25 to 0.02.*

removing all but 2% of the errors in the ODE evaluation for the *Always-On* system. This enforces not only ordering between stages but also between different steps within a stage by making some reactions slower than others. Comparing to the *Timed* system variant, we see that here, the ordering issue is mitigated automatically via the added timing control. Even with set 1, there are no errors indicated by the ODE analysis, showing how the *Timed* variant provides simpler initial tuning and setup compared to the *Always-On* variant. However, as we will show in the following, the actual performance can only be determined through stochastic simulations and calculation of the input-weighted error probability P_e , as explained in Section V.

B. Stochastic Simulation and Impact of Bayesian Optimization

The parameters for stochastic evaluation used for all results shown in the following can be found in Table IV. Figure 18 shows the resulting probability of correct detection $P_d[N(Y_{\text{on}})]$ across the range of possible input values on the x -axis, as well as the input likelihood for reference in grey. The thick colored lines show the average value, while the shaded area is associated with the 95% CI. The blue line depicts P_d for the *Timed* variant using set 1, identified as error-free during the ODE tuning described above in Figure 17. The results show that while the average value of P_d largely remains above 50%, as indicated by the ODE analysis, there are large parts of the input space with P_d at or close to 50%. The input-weighted error probability is $P_e = 0.25$. This means that in this configuration ChemSICal-Net does not align with the desired algorithm behavior in many cases that occur with high likelihood. The red line in Figure 18 depicts $P_d[N(Y_{\text{on}})]$ after we have applied our proposed adaptive BO scheme, using the setup and parameters described in Section VI. We can see that the performance can be significantly increased across the entire range of input values with a particular emphasis on the most likely regions. P_d retains the characteristic shape with peaks and minima roughly in the same places where the input likelihood has peaks and minima. This is caused by the correct choice of threshold concentrations and is very advantageous

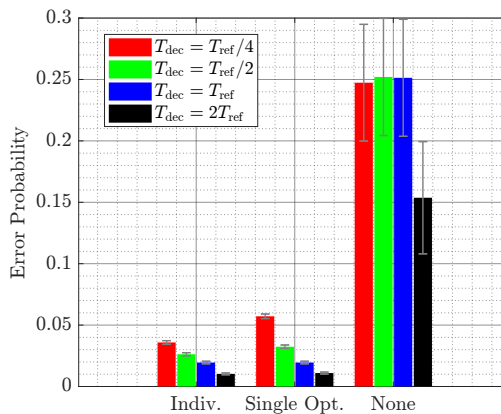


Fig. 19: Comparison of the input-weighted error probability P_e for different decision time horizons T_{dec} and different optimization configurations. For *Indiv. Opt.*, BO scheme is run for each value of T_{dec} individually. For *Single Opt.*, BO is only run for $T_{\text{dec}} = T_{\text{ref}}$ and results applied to all other values of T_{dec} . For *None*, parameters correspond to set 1 in Table V. *BO improves P_e across all T_{dec} ; individual tuning matters most for short T_{dec} .*

towards reducing the input-weighted error probability, since the input regions with the lowest P_d also have the lowest likelihood. Overall, the application of the BO scheme reduces P_e from 0.25 to ≈ 0.02 .

To investigate the impact of optimization further, we incorporate different values of the decision time horizon T_{dec} and two different optimization configurations. We denote the case, where we individually run the BO scheme for each value of T_{dec} as *Indiv. Opt.*. We further perform an analysis, where we only optimize the parameters for $T_{\text{dec}} = T_{\text{ref}}$ once, and then apply those same parameters for all other values of T_{dec} . This is denoted as *Single Opt.*. When we use the parameters from ODE tuning, we denote this optimization configuration as *None*. The results are shown in Figure 19 with P_e on the y -axis and the values depicted as bars with a 95% CI. We can see that *Indiv. Opt.* with the BO scheme improves P_e by about one order of magnitude across all values of T_{dec} . Between the different decision times, i.e. larger T_{dec} means more time to decide, we can see that P_e and T_{dec} are directly connected. The lowest error probability is achieved, when ChemSICal-Net has the largest amount of decision time $T_{\text{dec}} = 2T_{\text{ref}}$, creating a clear trade-off between detection accuracy and decision time. Comparing between *Indiv. Opt.* and *Single Opt.*, we can see that tailoring the parameters specifically for one value of T_{dec} improves the performance further. However, the benefit becomes larger for shorter decision times T_{dec} .

C. Impact of Timing Control

In Figure 20, comparison results are presented for the stochastic evaluation of the *Timed* and *Always-On* variants after applying the BO scheme to both. The initial parameters for the optimization are defined by the respective results of the ODE tuning above. Across the different values of T_{dec} a trend emerges. We can observe a middle region, i.e. $T_{\text{dec}} = T_{\text{ref}}$, and $T_{\text{dec}} = T_{\text{ref}}/2$, where both variants perform relatively similar with a slight advantage for the *Timed* variant but within the CI. For the fast-decision case, i.e. $T_{\text{dec}} = T_{\text{ref}}/4$, the *Timed* variant clearly outperforms the *Always-On* variant by approximately a factor of 2. This demonstrates the ability

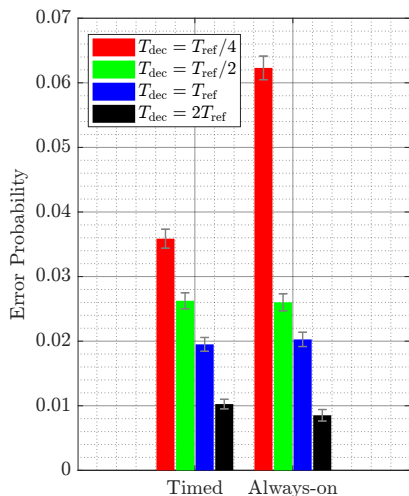


Fig. 20: Comparison of the input-weighted error probability P_e for different decision time horizons T_{dec} and two variants of ChemSICal-Net. For *Timed*, the chemical clock is used to gate the different stages. For *Always-On*, no clock gating is applied. *Timing helps for short T_{dec} ; for longer horizons, less overhead is preferable.*

of the timing control to separate computing steps in faster-paced environments. In contrast, for long decision times, i.e. $T_{dec} = 2T_{ref}$, the results show a small but visible advantage for the *Always-On* scheme by a factor of 1.2. In this regime, the ChemSICal-Net system has a long time for any molecule species to converge to correct values and also correct initial wrong decisions over time, so that the issues with premature decisions outlined in Section IV are not as relevant. At the same time, the addition of more reactions and gating effects in the *Timed* variant cause more variance and distortion to the intended reaction block operation. This causes a slightly higher error rate.

D. Relation to the Analytical System

In our previous work [8], [37], we have proposed and analyzed a non-chemical version of the SIC algorithm for DBMC-NOMA. The channel model and communication system assumptions were identical to the ones utilized in this paper so that the results are comparable. In the computationally accurate implementation without CRNs, the derived analytical model predicts an error probability of approximately 10^{-6} , i.e. four orders of magnitude smaller than the smallest reported P_e by the ChemSICal-Net system for the longest decision time T_{dec} . This highlights the fact that the chemical implementation of an algorithm designed for DBMC systems will most likely dominate the error characteristic of the system over the inherent error generated by the channel noise and modulation and detection scheme [13]. As a result, an improvement in the error probability of the chemical implementation will directly translate into performance gains of the entire system and, therefore, the consideration of the chemical aspects should be prioritized. Additionally, the propagation and computation time will similarly be dominated by the chemical reaction dynamics. Although we use normalized reaction speeds in this work, realistic time scales for appropriate reactions like enzyme- or DNA strand-based systems are on the order of minutes [23], [42], while diffusion transport over micro- or nanoscale distances, or flow-based transport across larger

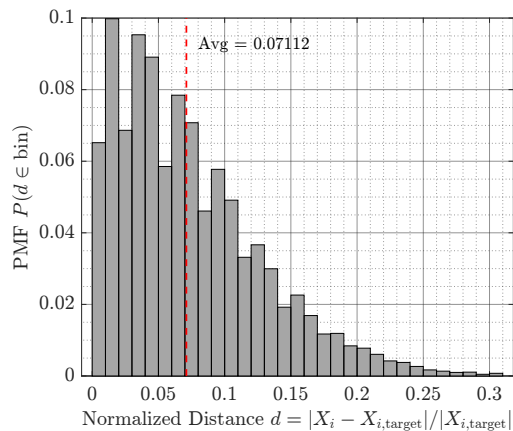


Fig. 21: Plot evaluating the success of the reset mechanism. The figure shows a binned probability mass function of the relative normalized distance of the X comparison species from its respective target value after reset.

distances can take below one second to several seconds [43]. Therefore, reducing the decision time of the CRN system by appropriate tuning of the reaction parameters will be crucial.

E. Proof-of-Concept Extensions

Lastly, we want to highlight the results of our preliminary extensions of the ChemSICal-Net system, which showcase the potential for scaling and implementation as well as future challenges that need to be addressed.

1) Reset Mechanism

For our evaluation of the ChemSICal-Net+R reset mechanism, we performed stochastic simulations of the standard ChemSICal-Net reaction network across the entire input range and added the reset phase at the end. Thereby, the molecule species ended up in various possible constellations before having to be reset to the target values. Additionally, we applied our BO scheme to optimize the parameters of the reset mechanism. The results showed that the RRCs controlling the individual reset reactions should be set to $\kappa_{\max} = 1$, i.e. as fast as possible. In any case, due to the simplicity of the reactions, the reset process takes much less time than the SIC decision time, with $T_R \ll T_{dec}$.

The decision species D_i^0 and D_i^1 , as well as other intermediate species must return to zero molecule count. In our evaluation, this was successful in all simulated trajectories. The intermediate species $X_{\text{off},i}$ and $X_{\text{on},i}$ encode the threshold adaptation values for the SIC decision tree and need to return to their original non-zero values. In Figure 21, we show a binned probability mass function over the relative normalized distances of all X species from their target at the end of the reset period T_R . We can see that the species count deviated on average by about 7% from the targets, while 95% of species returned to within 20% of their target. The reset mechanism, therefore, works in principle, but should be tuned and evaluated further in future work.

2) Adding a Third TX

For this evaluation, we set up the system as described in Section IV-B1 to add another TX to the SIC decoding process. We run stochastic simulations with the standard parameters, as in Table IV and apply our BO scheme to optimize the CRN parameters. Here, we only looked at the case where

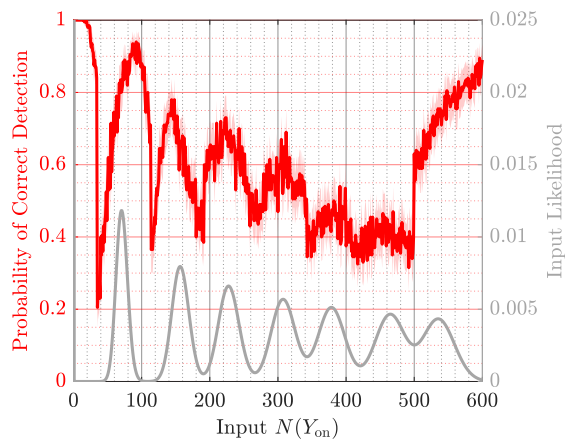


Fig. 22: Plot of P_d in red for the extension with an additional TX. Input likelihood for the 3-TX case is shown in grey.

$T_{\text{osc}} = 2T_{\text{ref}}$. For the 3-TX variant we set $T_{\text{osc}} = \frac{3}{2}T_{\text{dec}}$, so that three half-cycles of the oscillation are contained within T_{dec} to represent the three stages. Figure 22 depicts the resulting P_d and the input likelihood. It is clearly visible that the input likelihood $p_{n_s}[N(Y_{\text{on}})]$ is different from the 2-TX case due to the larger number of possible symbol combinations of the three TXs. The plotted P_d exhibits the same characteristic shape as before, where the peaks and minima line up with the likelihood. However, in this case, the input likelihood does not have the same pronounced minima as the 2-TX system, making it difficult to avoid the strong influences of dips in the detection accuracy between two peaks and causing a lower accuracy overall. We observe a significant symbol-combination dependence of the detection accuracy, where symbols with higher arriving molecule count result in a lower accuracy. This scenario reveals one of the drawbacks of the efficiency-focused input sampling for the optimization scheme. As we are only considering the likelihood peaks for the optimization, the minima are not considered. However, in the final evaluation they have a much larger influence due to the shape of the input likelihood in this case. In the future, the optimization should be tuned to take into account more values close to the midpoints between peaks given that there is more time and computing power available. In general, the mechanism to expand the number of TXs is functional and structurally sound and exhibits sub-exponential complexity scaling as explained in Section IV-B1. Future evaluations should look into the molecule counts necessary to make larger numbers of TXs viable with higher detection accuracy.

VIII. CONCLUSION AND FURTHER WORK

This work presented ChemSICal-Net, an end-to-end chemical RX framework that realizes SIC-based multi-user reception for DBMC MA using a stochastic CRN. We mapped the algorithmic SIC pipeline to modular reaction blocks, introduced oscillator-based timing control to gate multi-stage processing, and integrated an adaptive BO scheme to tune constrained RRCs with communication-centric objectives that improved error probability from the non-optimized baseline by one order of magnitude. Performance was evaluated using deterministic ODE analysis and MCS based on stochastic sim-

ulation trajectories, highlighting how timing control reduced error probability by 2x for short decision time horizons, and showing that a non-clocked design can be beneficial due to lower reaction overhead. In addition, we provided an explicit benchmarking comparison across oscillator model families and optimization schemes, which clarifies and motivates the design choices made for ChemSICal-Net.

Key limitations concern the overall CRN complexity and the accuracy and portability of kinetic parameters, the currently abstracted channel-to-CRN interface, i.e. sample-and-hold of the received observation, and the practical feasibility and time-scale of the oscillator implementation. Next, we will investigate implementations of the proposed chemical circuits using DNA strand displacement, leveraging our microfluidic interaction-channel platform [23], and extend the framework to larger numbers of TXs by expanding the control mechanism through timing and multi-species oscillator designs.

REFERENCES

- [1] N. Farsad, H. B. Yilmaz, A. Eckford, C.-B. Chae, and W. Guo, "A Comprehensive Survey of Recent Advancements in Molecular Communication," *IEEE Commun. Surv. Tutor.*, vol. 18, no. 3, 2016.
- [2] V. Jamali, A. Ahmadzadeh, W. Wicke, A. Noel, and R. Schober, "Channel Modeling for Diffusive Molecular Communication—A Tutorial Review," *Proc. IEEE*, vol. 107, no. 7, Jul. 2019.
- [3] I. F. Akyildiz, M. Pierobon, S. Balasubramaniam, and Y. Koucheryav, "The Internet of Bio-Nano Things," *IEEE Commun. Mag.*, vol. 53, no. 3, Mar. 2015.
- [4] F. C. Landers, L. Hertle, V. Pustovalov, D. Sivakumaran, C. M. Oral *et al.*, "Clinically ready magnetic microrobots for targeted therapies," *Science*, vol. 390, no. 6774, Nov. 2025.
- [5] Y. Elani, R. V. Law, and O. Ces, "Vesicle-based artificial cells as chemical microreactors with spatially segregated reaction pathways," *Nature Communications*, vol. 5, no. 1, Oct. 2014.
- [6] E. Shitiri and H.-S. Cho, "A TDMA-Based Data Gathering Protocol for Molecular Communication via Diffusion-Based Nano-Sensor Networks," *IEEE Sensors J.*, vol. 21, no. 17, Sep. 2021.
- [7] J. Wang, S. Ögüt, H. Al Hassanieh, and B. Krishnaswamy, "Towards Practical and Scalable Molecular Networks," in *Proc. ACM SIGCOMM*, Sep. 2023.
- [8] A. Wietfeld, S. Schmidt, and W. Kellerer, "DBMC-NOMA: Evaluating NOMA for Diffusion-Based Molecular Communication Networks," in *Proc. IEEE ICC*, Jun. 2024.
- [9] M. Vasić, D. Soloveichik, and S. Khurshid, "CRN++: Molecular programming language," *Natural Computing*, vol. 19, no. 2, Jun. 2020.
- [10] D. Bi, Y. Deng, M. Pierobon, and A. Nallanathan, "Chemical Reactions-Based Microfluidic Transmitter and Receiver Design for Molecular Communication," *IEEE Trans. Commun.*, vol. 68, no. 9, Sep. 2020.
- [11] V. Walter, D. Bi, A. Salehi-Reyhani, and Y. Deng, "Real-time signal processing via chemical reactions for a microfluidic molecular communication system," *Nature Communications*, vol. 14, no. 1, Nov. 2023.
- [12] B. Heinlein, L. Brand, M. Egan, M. Schäfer, R. Schober, and S. Lotter, "Closing the Implementation Gap in MC: Fully Chemical Synchronization and Detection for Cellular Receivers," *IEEE Trans. Mol. Biol. Multi-Scale Commun.*, vol. 11, no. 1, Mar. 2025.
- [13] A. Wietfeld, M. Wendrich, S. Schmidt, and W. Kellerer, "ChemSICal: Evaluating a Stochastic Chemical Reaction Network for Molecular Multiple Access," in *Proc. IEEE ICC*, Jun. 2025.
- [14] B. J. Shields, J. Stevens, J. Li, M. Parasram, F. Damani, J. I. M. Alvarado, J. M. Janey, R. P. Adams, and A. G. Doyle, "Bayesian reaction optimization as a tool for chemical synthesis," *Nature*, vol. 590, no. 7844, Feb. 2021.
- [15] E. Braconi, "Bayesian optimization as a valuable tool for sustainable chemical reaction development," *Nature Reviews Methods Primers*, vol. 3, no. 1, pp. 1–2, Oct. 2023.
- [16] J. Guo, B. Ranković, and P. Schwaller, "Bayesian Optimization for Chemical Reactions," *CHIMIA*, vol. 77, no. 1/2, Feb. 2023.
- [17] X. Chen, M. Wen, C.-B. Chae, L.-L. Yang, F. Ji, and K. K. Igvovich, "Resource Allocation for Multiuser Molecular Communication Systems Oriented to the Internet of Medical Things," *IEEE Internet Things J.*, vol. 8, no. 21, Nov. 2021.

- [18] V. Jamali, H. M. Loos, A. Buettner, R. Schober, and H. Vincent Poor, "Olfaction-inspired MCs: Molecule Mixture Shift Keying and Cross-Reactive Receptor Arrays," *IEEE Trans. Commun.*, vol. 71, no. 4, Apr. 2024.
- [19] Y. Saito, Y. Kishiyama, A. Benjebbour, T. Nakamura, A. Li, and K. Higuchi, "Non-Orthogonal Multiple Access (NOMA) for Cellular Future Radio Access," in *2013 IEEE Proc. 77th Veh. Technol. Conf. (VTC Spring)*, Dresden, Germany, Jun. 2013.
- [20] A. Wietfeld, S. Schmidt, and W. Kellerer, "Error Probability Optimization for Non-Orthogonal Multiple Access in DBMC Networks," *IEEE Trans. Mol. Biol. Multi-Scale Commun.*, vol. 10, no. 3, Sep. 2024.
- [21] S. Angerbauer, W. Haselmayr, F. Enzenhofer, T. Pankratz, R. Khanzadeh, and A. Springer, "Molecular Nano Neural Networks (M3N): In-Body Intelligence for the IoBNT," in *Proc. IEEE ICC*, Jun. 2024.
- [22] F. Lau, S. Scheer, A. Waldner, and S. Fischer, "Communication Protocols for Molecular Communication Networks Based on DNA," in *Proc. ACM NANOCOM*, Oct. 2024.
- [23] A. Wietfeld, A. Bienau, F. C. Simmel, and W. Kellerer, "Modeling the Microfluidic Interaction Channel for DNA-Based Molecular Communication Experiments," in *Proc. ACM NANOCOM*, Oct. 2025.
- [24] H. Jiang, M. Riedel, and K. Parhi, "Synchronous sequential computation with molecular reactions," in *Proc. DAC '11*. ACM, Jun. 2011.
- [25] H. Jiang, A. P. Kharam, M. D. Riedel, and K. K. Parhi, "A synthesis flow for digital signal processing with biomolecular reactions," in *Proc. IEEE/ACM ICCAD*, Nov. 2010.
- [26] X. Shi and C. Gao, "Design of Universal Chemical Relaxation Oscillator to Control Molecular Computation," *SSRN E-Journal*, 2022.
- [27] L. Cardelli and A. Csikász-Nagy, "The Cell Cycle Switch Computes Approximate Majority," *Scientific Reports*, vol. 2, no. 1, Sep. 2012.
- [28] T. Y.-C. Tsai, Y. S. Choi, W. Ma, J. R. Pomeroy, C. Tang, and J. E. Ferrell, "Robust, tunable biological oscillations from interlinked positive and negative feedback loops," *Science*, vol. 321, no. 5885, Jul. 2008.
- [29] T. Suwanmajo and J. Krishnan, "Mixed mechanisms of multi-site phosphorylation," *J. R. Soc. Interface*, vol. 12, 06 2015.
- [30] B. Jiang, W. Yu, and L. Lin, "Clock Signal Generation for IoBNT Using Self-Sustaining Oscillations via Protein Circuit Design," *IEEE Internet of Things J.*, 2025.
- [31] M. Vasić, C. Chalk, A. Luchsinger, S. Khurshid, and D. Soloveichik, "Programming and training rate-independent chemical reaction networks," *PNAS*, vol. 119, no. 24, Jun. 2022.
- [32] N. Murphy, R. Petersen, A. Phillips, B. Yordanov, and N. Dalchau, "Synthesizing and tuning stochastic chemical reaction networks with specified behaviours," *J. R. Soc. Interface*, vol. 15, no. 145, Aug. 2018.
- [33] C. P. Robert and G. Casella, *Monte Carlo Statistical Methods*, ser. Springer Texts in Statistics. New York, NY: Springer, 2004.
- [34] J. H. Kalivas, *Adaption of Simulated Annealing to Chemical Optimization Problems*. Elsevier, Aug. 1995.
- [35] M. Ashyraliyev, Y. Fomekong-Nanfack, J. A. Kaandorp, and J. G. Blom, "Systems biology: Parameter estimation for biochemical models," *The FEBS Journal*, vol. 276, no. 4, Feb. 2009.
- [36] J. Torres Gómez, K. Pitke, L. Stratmann, and F. Dressler, "Age of information in molecular communication channels," *Digital Signal Processing*, May 2022.
- [37] A. Wietfeld and W. Kellerer, "DBMC-aNOMaLy: Asynchronous NOMA with Pilot-Symbol Optimization Protocol for Diffusion-Based Molecular Communication Networks," Dec. 2025, arXiv:2512.07317.
- [38] J. H. Abel, B. Drawert, A. Hellander, and L. R. Petzold, "GillesPy: A Python Package for Stochastic Model Building and Simulation," *IEEE Life Sciences Letters*, vol. 2, no. 3, Sep. 2016.
- [39] L. Cardelli, R. D. Hernansaiz-Ballesteros, N. Dalchau, and A. Csikász-Nagy, "Efficient Switches in Biology and Computer Science," *PLOS Computational Biology*, vol. 13, no. 1, Jan. 2017.
- [40] M. B. Elowitz and S. Leibler, "A synthetic oscillatory network of transcriptional regulators," *Nature*, vol. 403, no. 6767, Jan. 2000.
- [41] C. Conradi, M. Mincheva, and A. Shiu, "Emergence of Oscillations in a Mixed-Mechanism Phosphorylation System," *Bull. Math. Biol.*, vol. 81, no. 6, Jun. 2019.
- [42] B. N. Kholodenko, "Negative feedback and ultrasensitivity can bring about oscillations in the mitogen-activated protein kinase cascades," *Eur. J. Biochem.*, vol. 267, no. 6, Mar. 2000.
- [43] A. Wietfeld, S. Schmidt, and W. Kellerer, "Evaluation of a Multi-Molecule Molecular Communication Testbed Based on Spectral Sensing," in *Proc. IEEE GLOBECOM*, Dec. 2024.